Acta Crystallographica Section D
Biological Crystallography
ISSN 0907-4449

Structure of the human p53 core domain in the absence of DNA

Ying Wang,[a] Anja Rosengarth[a] and Hartmut Luecke[a,b,c]*

[a]Department of Molecular Biology and Biochemistry, 3205 McGaugh Hall, University of California, Irvine, CA 92697-3900, USA, [b]Department of Physiology and Biophysics, University of California, Irvine, CA 92697, USA, and [c]Department of Computer Science, University of California, Irvine, CA 92697, USA

Correspondence e-mail: hudel@uci.edu

Received 28 September 2006
Accepted 14 November 2006

PDB Reference: human p53 core domain, 2ocj, r2ocjsf.

The tumor suppressor protein p53 plays a key role in cell-cycle regulation by triggering DNA repair, cell-cycle arrest and apoptosis when the appropriate signal is received. p53 has the classic architecture of a transcription factor, with an amino-terminal transactivation domain, a core DNA-binding domain and carboxy-terminal tetramerization and regulatory domains. The crystal structure of the p53 core domain, which includes the amino acids from residue 96 to residue 289, has been determined in the absence of DNA to a resolution of 2.05 Å. Crystals grew in a new monoclinic space group ($P2_1$), with unit-cell parameters $a = 68.91$, $b = 69.36$, $c = 84.18$ Å, $\beta = 90.11^\circ$. The structure was solved by molecular replacement and has been refined to a final R factor of 20.9% ($R_{\rm free}$ = 24.6%). The final model contains four molecules in the asymmetric unit with four zinc ions and 389 water molecules. The non-crystallographic tetramers display different protein contacts from those in other p53 crystals, giving rise to the question of how p53 arranges as a tetramer when it binds its target DNA.

1. Introduction

p53 has been described as playing the 'nemesis' to most cancers (Bullock & Fersht, 2001). It is activated in response to certain stressful situations, such as DNA damage, oncogene activation and chemotherapy. Specific post-translational modifications stabilize p53 and promote sequence-specific DNA binding (Lavin & Gueven, 2006). The transcription products of p53 target genes such as p21, FAS, GADD45, *etc.* directly elicit cell-cycle checkpoints and apoptosis (Bullock & Fersht, 2001).

The full-length p53 molecule is comprised of three major domains: the N-terminal transactivation domain, the core DNA-binding domain and the C-terminal tetramerization domain. p53 is mutated in about half of all human cancers, with 95% of these mutations occurring in the core domain (Vousden & Lu, 2002). Thermodynamic studies of p53 cancer mutants have identified three major phenotypes classified as (i) mutations affecting DNA contacts that have little impact on protein folding, (ii) mutations disordering the local structure (*e.g.* destabilized relative to the wild type by <2 kcal mol^{-1}, thus leaving p53 >85% folded) and (iii) mutations globally denaturing the core domain (*e.g.* destabilized by >3 kcal mol^{-1}, thus resulting in >50% unfolded p53; Bullock *et al.*, 1997, 2000; Nikolova *et al.*, 1998; Wong *et al.*, 1999) (1 kcal = 4.184 kJ).

The high level of accumulated mutant p53 in tumor cells makes p53 a promising target for pharmacological therapeutic intervention, with the aim of refolding inactive p53 into its active conformation (Brachmann, 2004). The feasibility of this strategy has been demonstrated by applying small-molecule

Table 1
Data-collection and refinement statistics.

Values in parentheses are for the highest resolution shell.

Space group	$P2_1$
Unit-cell parameters (Å, °)	a = 68.91, b = 69.36, c = 84.18, β = 90.11
Resolution (Å)	50–2.05 (2.12–2.05)
Unit-cell volume (Å^3)	402346
V_M (Å^3 Da^{-1})	2.05
Solvent content (%)	40.0
Protein molecules per ASU	4
Observed reflections	187663
Unique reflections	49562
Completeness (%)	99.1 (98.4)
$I/\sigma(I)$	26.4 (6.7)
Redundancy	3.8 (3.7)
R_{merge}† (%)	16.2 (53.5)
Mosaicity (°)	0.45
Refinement	
Protein atoms	6096 (4 molecules)
Zinc ions	4
Water molecules	389
Resolution range (Å)	50.0–2.05 (2.06–2.05)
R‡ (%)	20.9 (23.9)
R_{free}§ (%)	24.6 (29.7)
R.m.s.d. bond lengths (Å)	0.006
R.m.s.d. bond angles (°)	1.27
Ramachandran plot	
Residues in core regions (%)	88.5
Residues in additional allowed regions (%)	11.2
Residues in generously allowed regions (%)	0.3
Residues in disallowed regions (%)	0.0

† $R_{merge} = \sum_h \sum_i |I_{h,i} - \langle I_h \rangle| / \sum_h \sum I_{h,i}$, where $\langle I_h \rangle$ is the mean intensity of symmetry-related reflections, $I_{h,i}$. ‡ $R = \sum ||F_o| - |F_c|| / \sum |F_o|$, where F_o and F_c are the observed and calculated structure-factor amplitudes, respectively. § R_{free} was calculated for 9.2% of the data that were withheld from refinement.

compounds *in vitro* or *in vivo* to yield rescue results (Bykov *et al.*, 2003). A possible drug rescue mechanism is based on the hypothesis that an equilibrium exists between the distorted/denatured and the native-state p53 core domain structures, as well as between the unbound native-state and DNA-bound-state p53 (Bullock & Fersht, 2001). Drugs that selectively bind to the population with the native-state structure of the mutant shift the equilibrium in favor of the native state, thus restoring wild-type function. According to this model, potential drugs should preferentially bind to the native p53 structure. To rescue cancer mutations in the β-sandwich using this strategy appears appealing, given the fact that 25% of p53 missense mutations fall into this region (Vousden & Lu, 2002).

Oligomerization of full-length p53 is critical for DNA binding based on the evidence that monomeric p53 does not bind to DNA, while dimeric and tetrameric p53 do so *in vitro* (Shaulian *et al.*, 1993; Tarunina & Jenkins, 1993; Zhang *et al.*, 1994; Waterman *et al.*, 1995). Electron microscopy revealed that an entire p53 tetramer connects two separate consensus sites together *in vitro* (Jackson *et al.*, 1998; Wang *et al.*, 1994). The crystal structure of the p53 C-terminal tetramerization domain shows that four monomers generate a fourfold helix bundle in the crystal (Jeffrey *et al.*, 1995; Mittl *et al.*, 1998). Therefore, it is inferred that the oligomeric form of full-length p53 is a tetramer in the presence of DNA in solution. In addition, numerous structural analyses have been explored to propose models of the p53–DNA complex (Cho *et al.*, 1994; Klein *et al.*, 2001; Kitayner *et al.*, 2006). All results are in agreement that full-length p53 forms a tetramer and that all four monomers are responsible for the sequence-specific recognition of the DNA-binding site.

In this study, we present the crystal structure of the human wild-type p53 core domain in the absence of DNA, which causes new tetrameric arrangements. This structure is an important control for p53 mutants (cancer as well as rescue mutants) and may also serve as a potential binding target for small molecules in virtual ligand screening studies.

2. Materials and methods

2.1. Purification and crystallization of the wild-type p53 core domain

The plasmid carrying the DNA sequence encoding the wild-type p53 core domain (residues 94–312) was transformed into *Escherichia coli* BL21 (DE3) strain. Cells were grown at 310 K to an OD_{600} of 0.6 prior to overnight induction with 0.5 m*M* IPTG (isopropyl β-D-thiogalactoside) at 293 K (Bullock *et al.*, 1997). The cells were isolated by centrifugation and lysed in 50 m*M* imidazole pH 7.2, 5 m*M* dithiothreitol (DTT), 1 m*M* phenylmethylsulfonyl fluoride (PMSF) using a French press. The supernatant was loaded onto a SP-Sepharose cation-exchange column (Pharmacia) and eluted with an NaCl gradient (0–600 m*M*). The eluted fractions were pooled and dialyzed against 50 m*M* imidazole pH 7.2, 5 m*M* DTT. Further purification was achieved by affinity chromatography using a HiTrap heparin Sepharose column in 50 m*M* imidazole pH 7.2, 5 m*M* DTT with an NaCl gradient (0–600 m*M*), followed by dialysis against 20 m*M* Tris pH 7.6, 150 m*M* NaCl, 10 m*M* DTT. Columns were kept at 277 K. Pure protein was concentrated and the concentration was determined with a spectrophotometer using an extinction coefficient of ε_{280} = 16 920 cm^{-1} M^{-1} as calculated by the method of Gill & von Hippel (Gill & von Hippel, 1989). Aliquots were stored at 253 K until further use.

Crystals were grown in the absence of DNA by using the sitting-drop vapor-diffusion technique at room temperature (Joerger *et al.*, 2004). 2 µl protein solution (5 mg ml^{-1} protein in 20 m*M* Tris pH 7.6, 150 m*M* NaCl, 10 m*M* DTT) was mixed with 2 µl reservoir buffer consisting of 100 m*M* HEPES pH 7.6, 10 m*M* DTT and 14–21%(*w*/*v*) polyethylene glycol (PEG) 4000 and equilibrated against 500 µl reservoir buffer. Colorless plate-shaped crystals were obtained within a few days. Crystals were flash-cooled in cryo-buffer consisting of 100 m*M* HEPES pH 7.6, 35%(*w*/*v*) PEG 4000 and 300 m*M* NaCl.

2.2. Data collection and structure determination

A diffraction data set from crystals of the wild-type p53 core domain was collected to 2.05 Å resolution at 100 K on beamline 5.0.2 at the Advanced Light Source (ALS), Berkeley, CA, USA. The data set was indexed, integrated and further processed using *HKL*-2000 (Otwinowski & Minor, 1997). The crystal belongs to a new space group ($P2_1$). A total of 9.2% of all reflections were flagged for the calculation of

R_{free} and were excluded from subsequent refinement. Data-collection statistics are shown in Table 1.

The structure was solved by molecular replacement with the program *Phaser* using diffraction data in the range 50–2.05 Å (Storoni *et al.*, 2004). Molecule *B* of DNA-bound wild-type p53 (PDB code 1tsr) was used as the search model (Cho *et al.*, 1994) to locate the orientations and positions of four independent copies of the core domain in the asymmetric unit. Rigid-body refinement, simulated annealing and restrained individual isotropic *B*-factor refinement were carried out with *CNS* (Brünger *et al.*, 1998). Models were manually rebuilt using $2F_o - F_c$ and $F_o - F_c$ maps using the program *O* (Jones *et al.*, 1991). Water molecules were introduced into the structure using the automatic water-picking routine of *CNS* (Brünger *et al.*, 1998). One zinc ion per monomer was inserted at the site formed by residues Cys176, Cys238, Cys242 and His179. Since the residues at the very N- and C-termini are disordered, two amino acids at the N-terminus and 23 at the C-terminus are not visible in the electron-density map. Therefore, the atomic model comprises residues 96–289. The refinement statistics are summarized in Table 1. *PROCHECK* was used to validate the stereochemistry (Laskowski *et al.*, 1996). Figures were generated with *PyMOL* (DeLano, 2002) and *Swiss-PdbViewer* (Guex & Peitsch, 1997).

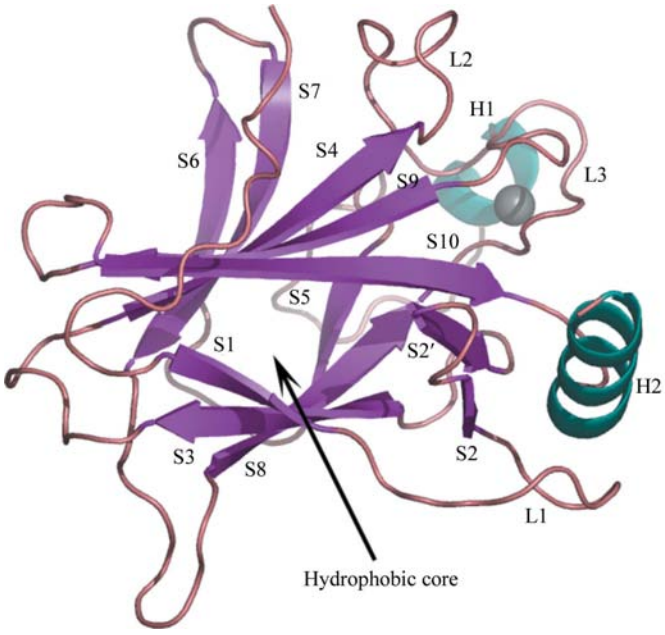

Figure 1
Schematic ribbon diagram of the overall structure of the p53 core domain in the absence of DNA. The zinc ion is highlighted in dark gray near loop L3.

3. Results and discussion

3.1. Overall structure of the DNA-free human p53 core domain

DNA-free p53 crystals belong to a new space group ($P2_1$) with four molecules in the asymmetric unit. The overall structure of each of the four monomers is very similar to that of wild-type p53 in complex with DNA (Fig. 1). Each core domain monomer is comprised of an immunoglobulin-like β-sandwich consisting of two twisted antiparallel β-sheets of four (S1, S3, S8 and S5) and five (S10, S9, S4, S7 and S6) strands, with these two sheets packing together into a β-sandwich, forming a hydrophobic inner core. The DNA-binding surface, which includes two large loops (L2 and L3) and a loop–sheet–helix motif, is located at one end of the β-sandwich architecture. A zinc ion is tetrahedrally coordinated by Cys176, His179, Cys238 and Cys242, where it stabilizes the two large loops (L2 and L3) involved in DNA binding. The loop–sheet–helix motif comprises loop L1, the S2–S2′ hairpin and the C-terminal residues of the extended β-strand S10 and helix H2.

Superposition of the four molecules of the wild-type p53 core domain in the asymmetric unit reveals root-mean-square deviations (r.m.s.d.s) of 0.21, 0.30 and 0.46 Å (molecule *A* with molecules *B*, *C* and *D*, respectively) using all backbone atoms (Fig. 2). The major structural variations occur in the turn between strands S7 and S8 opposite the DNA-binding interface of the molecule, where the maximal distance between C^{α} atoms observed for Val225 is 3.8 Å, suggesting inherent flexibility in this region of the core domain. Recent research results illustrate the importance of the stability of this turn region: a *Caenorhabditis elegans* p53 mutant with a shortened turn between strands S7 and S8 had higher stability and the L1 loop was significantly stabilized (Pan *et al.*, 2006). Moreover, the newly determined structure of a rescued cancer mutant (V157F/N235K/N239Y) with the cancer mutation V157F together with the global suppressor motif N235K/N239Y

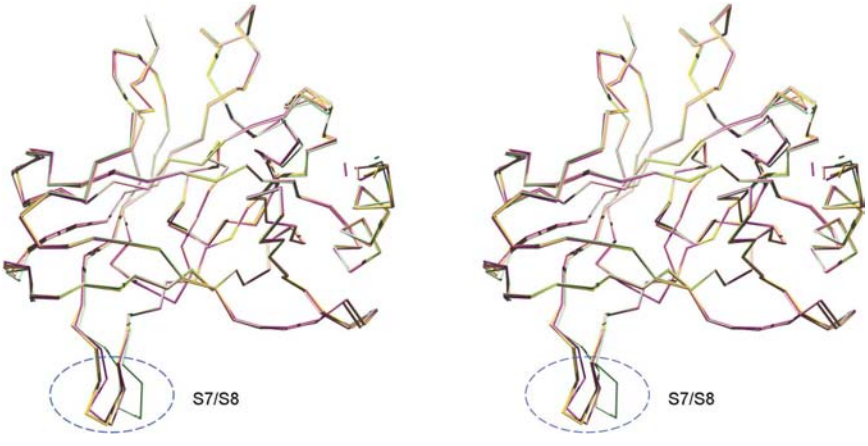

Figure 2
Backbone superposition of the four molecules in the asymmetric unit of the p53 core domain in the absence of DNA. Molecule *A*, yellow; molecule *B*, purple; molecule *C*, pink; molecule *D*, green. The region with the most significant structural variation is the turn between S7 and S8, which is encircled by a blue dashed line.

indicates that the S7/S8 turn region becomes even more flexible, with dramatically increased *B* factors (Luecke *et al.*, unpublished work).

Other regions with lower structural variability exist near the DNA-binding surface, including the L2 loop as well as the L3 loop, presumably owing to the inherent flexibility in the absence of DNA, although no direct contacts exist between these two loops and the DNA in 1tsr. In summary, when the four monomers in the asymmetric unit of the monoclinic form are compared, the S7/S8 turn stands out as the locus of highest structural variation; when comparison is made with a p53 monomer with bound DNA, it is one of three sites that show the most differences and is the only one that is distant from the DNA-binding site (see §3).

3.2. Gly245 is very important for the stability of the zinc-binding region

Recent statistical data on human p53 cancer mutants indicate that the top eight most frequent mutants alone account for 30% of the core domain single missense mutant pool, seven of which are mutations of arginines and the eighth one is G245S (which accounts for 2.23%; Brachmann, 2004). Those eight mutations are all clustered at or near the DNA-binding surface, either impairing direct DNA contacts or structurally disturbing the stability of the surrounding structure (Bullock *et al.*, 2000; Bullock & Fersht, 2001). Mutations at position 245 (a glycine in wild-type p53) were thought to induce conformational perturbation owing to increased side-chain length (Bullock *et al.*, 2000). However, careful analysis of the φ and ψ angles of Gly245 in the Ramachandran plot (both around -120°) suggests that no other amino acid can be accommodated at this position without distorting the main chain and thus the secondary structure (Cho *et al.*, 1994). Furthermore, a main chain-to-main chain hydrogen bond that stabilizes a tight turn (Gly245 NH to Cys242 C═O) is likely to be broken or weakened when position 245 contains a residue other than glycine. Cys242 is one of the zinc-coordinating residues (erroneously depicted as Cys247 in Cho *et al.*, 1994). The proximity of residue 245 to the zinc-coordinating cysteines Cys176 (loop L2) and Cys242 (loop L3) would be expected to result in mutation-induced distortions of the essential zinc-binding site. These observations help to explain the oncogenic mechanism of G245S and are further supported by an additional three p53 cancer mutants, G245D, G245C and G245V, all of which are ranked in the top 50 p53 cancer mutants.

3.3. Comparison with the human p53 core domain in complex with DNA

From the low structural differences between the four molecules within the asymmetric unit of the DNA-free form, it appears justified to take just one of the four molecules (such as molecule *A*) to represent the common characteristics. The same is the case for the three molecules of p53 crystallized in the presence of double-stranded DNA (0.69 Å r.m.s.d. between molecule *A* and molecule *B* and 0.73 Å r.m.s.d. between molecule *B* and molecule *C* by superimposing all backbone atoms), and thus it is reasonable to extract molecule *B* (the one with the most native-like DNA interactions) to represent the DNA-bound p53 structure (Cho *et al.*, 1994).

Structural comparison (backbone superposition) of the DNA-free p53 core domain structure (molecule *A*) with the DNA-bound p53 core domain structure (molecule *B* of 1tsr) results in an r.m.s.d. value of 0.68 Å (DNA-free p53 to DNA-bound p53; Fig. 3), which is only slightly higher than the overall structural deviations between the four independent monomers of the DNA-free form, suggesting that DNA binding does not significantly alter the structure of the p53 core domain. The largest differences between the DNA-free and the DNA-bound form occur in the loop regions L1 and L2 (loop L2 is at the back of the β-sandwich structure viewed in Fig. 3), which are likely to result from the absence of DNA and the inherent flexibility of these regions (Joerger *et al.*, 2004; Zhao *et al.*, 2001). Specifically, the C^{α} atom of Ser121 in the L1 loop is located about 5.1 Å from the equivalent position in the DNA-bound p53 structure and the C^{α} atom of the adjacent amino acid Lys120 is also displaced by 2.4 Å in the absence of DNA. In the complex of the wild-type p53 with consensus DNA, Lys120 contributes to DNA binding with two hydrogen bonds so as to fit the L1 loop into the major groove of DNA. Therefore, the L1 loop found in DNA-free p53 is not compatible with DNA binding and requires rearrangement to allow DNA binding. Part of the L2 loop shows another structural difference indicated by the position of the C^{α} atoms of Arg181–Gly187, in which the C^{α} atom of Arg183 is displaced by nearly 3.7 Å. Another structural deviation, which appears in the S7/S8 turn, is similar to those of

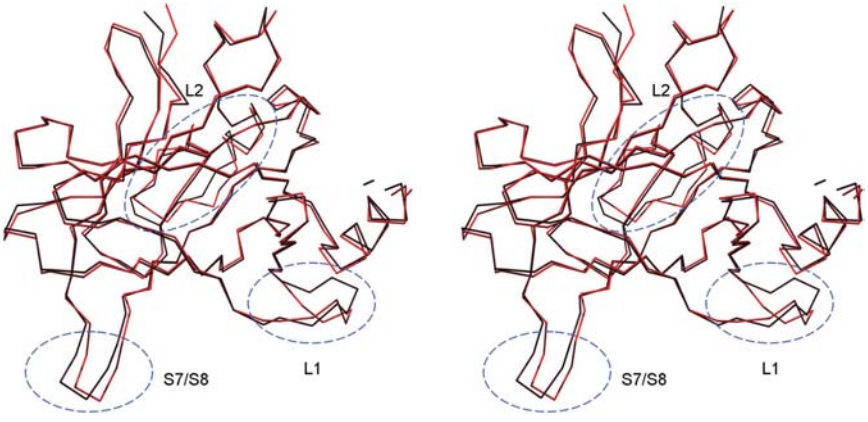

Figure 3
Backbone superposition of the DNA-free p53 core domain (molecule *A*, red) with DNA-bound p53 (1tsr, molecule *B*, black). The regions with the most significant structural variations are the turn between S7 and S8 as well as loops L1 and L2; these regions are encircled by blue dashed lines. Loop L2 is located at the bottom in this stereoview.

Table 2
Summary of different tetramers with their related molecules and contacts.

Tetramer No.	Contacts involved	Molecules involved
1	I, II, III and IV	*A*, *B*, *C* and *D*
2	III, IV, VII and VIII	*A*1, *B*1, *C* and *D*
3	I, II, V and VI	*A*2, *B*, *C*2 and *D*
4	V, VI, VII and VIII	*A*3, *B*1, *C*2 and *D*

Table 3
Summary of buried surface areas of different contacts.

Contact No.	Buried surface area (Å^2)	Molecules involved
I	254	*A* and *C*, *A*2 and *C*2
II	476	*B* and *D*
III	543	*A* and *B*, *A*1 and *B*1
IV	553	*C* and *D*
V	552	*A*2 and *B*, *A*3 and *B*1
VI	547	*C*2 and *D*
VII	486	*A*1 and *C*, *A*3 and *C*2
VIII	273	*B*1 and *D*

molecules related by non-crystallographic symmetry in the asymmetric unit and is likely to be caused by the different crystallographic environment and the inherent flexibility of this region. Noticeably, the S7/S8 turn is one of three sites that show the most structural differences and is the only one that is distant from the DNA-binding interface.

3.4. Crystal packing

The p53 core domain structure in the absence of DNA shows that four molecules, named *A*, *B*, *C* and *D*, form a non-crystallographic tetramer in the crystallographic *xz* plane (tetramer 1 in Table 2 and Fig. 4*a*). Those four molecules also contact neighboring molecules in the same layer perpendicular to the 2_1 (*y*) axis to form a total of four different types of tetramer; for instance, molecules *C*, *D*, *A*1 and *B*1 generate another non-crystallographic tetramer (tetramer 2 in Table 2 and Fig. 4*a*). None of these tetramers can be singled out as being the most energetically favorable based on intermolecular contact surface area. Intermolecular contacts and their respective buried surface areas are listed in Table 3. Most of the intermolecular contact areas are between 450 and 600 Å^2, except for contacts I and VIII (254 and 273 Å^2, respectively). Interestingly, DNA-binding-related segments L1 and H2 are directly involved in the contacts between molecules. For example, loop L1, helix H2 and the turn between S2 and S2′ of molecules *B* (and *D*) contact a pocket formed by S6 and S7 of molecules *A* (and *C*). In this arrangement, one of the p53 molecules would compete with DNA to bind to other p53 molecules, presumably resulting in a lowered affinity for DNA. Between layers, contacts between molecules appears to be insignificant (buried surface area data not shown here) owing to a large volume of disordered bulk solvent (Fig. 4*b*). All intermolecular contacts (from I to VIII) are different from those observed for the two types of dimer in DNA-bound human p53 (Cho *et al.*, 1994), the dimer of dimers reported for mouse p53 (Zhao *et al.*, 2001) and the head-to-tail dimer of the quadruple mutant M133L/V203A/N239Y/N268D in the absence of DNA (Joerger *et al.*, 2004). The strikingly different packing found in this new form of the p53 core domain raises the question whether there is only one tetrameric arrangement of p53 *in vivo* or whether there are

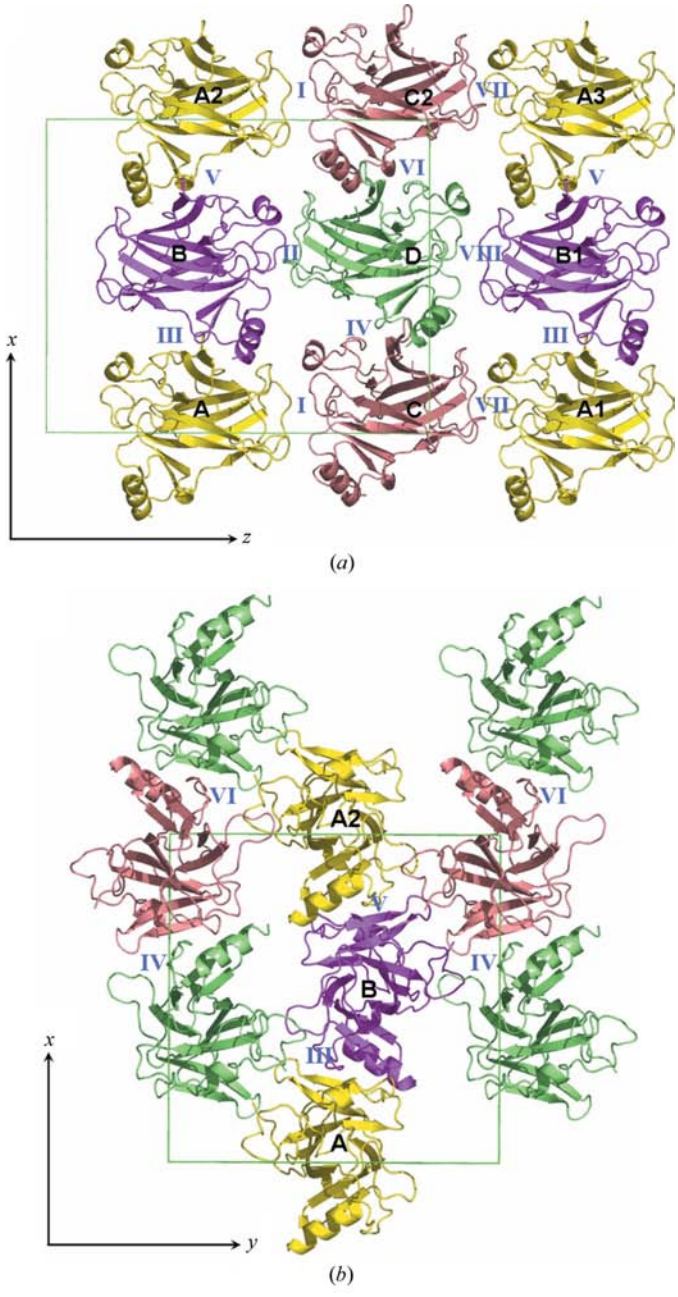

Figure 4
Crystal packing of the p53 core domain in the absence of DNA. (*a*) Top view of one layer of molecules in the *xz* plane. Molecules *A* and *C* (and molecules *B* and *D*) are related primarily *via* a translation in the *z* direction, coupled with an 18° rotation around an axis nearly parallel to the *x* axis (0.9946, −0.1032, −0.0101). Molecules *A* and *B* (and molecules *C* and *D*) are related by a rotation of 178° around an axis nearly parallel to the *z* axis (−0.0149, −0.1436, 0.9895). (*b*) Top view of molecules in the *xy* plane. The green box represents the dimensions of the $P2_1$ unit cell and Roman numerals indicate different crystal contacts. Different tetramers are formed by the four molecules in the asymmetric unit: *A*, yellow; *B*, purple; *C*, pink; *D*, green.

possibly competing multimerization mechanisms that result in different tetramers with distinct affinity for DNA or even with different DNA-binding modes. It has been shown that four monomers of the p53 C-terminal tetramerization domain (residues 325–355) form a tetramer (a dimer of dimers) in the crystal (Jeffrey *et al.*, 1995; Mittl *et al.*, 1998), while in our p53 core domain crystals no such symmetry is present. This leads to the conclusion that the p53 core-domain tetramers observed in the new monoclinic space group described herein are not compatible with the tetramer observed for the C-terminal tetramerization domain. Since only the p53 core domain and the C-terminal tetramerization domain by itself (Mittl *et al.*, 1998; Jeffrey *et al.*, 1995) have been determined structurally, further crystallographic studies are required to explore the structure of full-length p53, which may form a tetramer with different contacts owing to the participation of the transactivation and tetramerization domains.

4. Conclusion

We solved the structure of the human wild-type p53 core domain in the absence of DNA. Detailed analysis of non-crystallographic symmetry and crystal packing reveals that the p53 molecules are arranged differently from those in other p53 crystals, suggesting the existence of different p53 core domain tetramers. Furthermore, this new crystal form may be useful in structural studies of the binding modes of small molecules designed to stabilize the wild-type conformation of this crucial transcription factor.

We thank Dr Rainer Brachmann for generously providing the expression plasmid for the p53 core domain. We also thank Dr Don Senear and Dr Melanie Cocco for discussions. This research was supported by NIH grant R01-GM067808 and a UCI Chancellor's Fellowship.

References

Brachmann, R. K. (2004). *Cell Cycle*, **3**, 1030–1034.
Brünger, A. T., Adams, P. D., Clore, G. M., DeLano, W. L., Gros, P., Grosse-Kunstleve, R. W., Jiang, J.-S., Kuszewski, J., Nilges, M., Pannu, N. S., Read, R. J., Rice, L. M., Simonson, T. & Warren, G. L. (1998). *Acta Cryst.* D**54**, 905–921.
Bullock, A. N. & Fersht, A. R. (2001). *Nature Rev. Cancer*, **1**, 68–76.
Bullock, A. N., Henckel, J., DeDecker, B. S., Johnson, C. M., Nikolova, P. V., Proctor, M. R., Lane, D. P. & Fersht, A. R. (1997). *Proc. Natl Acad. Sci. USA*, **94**, 14338–14342.
Bullock, A. N., Henckel, J. & Fersht, A. R. (2000). *Oncogene*, **19**, 1245–1256.
Bykov, V. J., Selivanova, G. & Wiman, K. G. (2003). *Eur. J. Cancer*, **39**, 1828–1834.
Cho, Y., Gorina, S., Jeffrey, P. D. & Pavletich, N. P. (1994). *Science*, **265**, 346–355.
DeLano, W. L. (2002). *The PyMOL Molecular Graphics System.* http://www.pymol.org.
Gill, S. C. & von Hippel, P. H. (1989). *Anal. Biochem.* **182**, 319–326.
Guex, N. & Peitsch, M. C. (1997). *Electrophoresis*, **18**, 2714–2723.
Jackson, P., Mastrangelo, I., Reed, M., Tegtmeyer, P., Yardley, G. & Barrett, J. (1998). *Oncogene*, **16**, 283–292.
Jeffrey, P. D., Gorina, S. & Pavletich, N. P. (1995). *Science*, **267**, 1498–1502.
Joerger, A. C., Allen, M. D. & Fersht, A. R. (2004). *J. Biol. Chem.* **279**, 1291–1296.
Jones, T. A., Zou, J.-Y., Cowan, S. W. & Kjeldgaard, M. (1991). *Acta Cryst.* A**47**, 110–119.
Kitayner, M., Rozenberg, H., Kessler, N., Rabinovich, D., Shaulov, L., Haran, T. E. & Shakked, Z. (2006). *Mol. Cell*, **22**, 741–753.
Klein, C., Planker, E., Diercks, T., Kessler, H., Kunkele, K. P., Lang, K., Hansen, S. & Schwaiger, M. (2001). *J. Biol. Chem.* **276**, 49020–49027.
Laskowski, R. A., Rullmannn, J. A., MacArthur, M. W., Kaptein, R. & Thornton, J. M. (1996). *J. Biomol. NMR*, **8**, 477–486.
Lavin, M. F. & Gueven, N. (2006). *Cell Death Differ.* **9**, 941–950.
Mittl, P. R., Chene, P. & Grutter, M. G. (1998). *Acta Cryst.* D**54**, 86–89.
Nikolova, P. V., Henckel, J., Lane, D. P. & Fersht, A. R. (1998). *Proc. Natl Acad. Sci. USA*, **95**, 14675–14680.
Otwinowski, Z. & Minor, W. (1997). *Methods Enzymol.* **276**, 307–326.
Pan, Y., Ma, B., Levine, A. J. & Nussinov, R. (2006). *Biochemistry*, **45**, 3925–3933.
Shaulian, E., Zauberman, A., Milner, J., Davies, E. A. & Oren, M. (1993). *EMBO J.* **12**, 2789–2797.
Storoni, L. C., McCoy, A. J. & Read, R. J. (2004). *Acta Cryst.* D**60**, 432–438.
Tarunina, M. & Jenkins, J. R. (1993). *Oncogene*, **8**, 3165–3173.
Vousden, K. H. & Lu, X. (2002). *Nature Rev. Cancer*, **2**, 594–604.
Wang, P., Reed, M., Wang, Y., Mayr, G., Stenger, J. E., Anderson, M. E., Schwedes, J. F. & Tegtmeyer, P. (1994). *Mol. Cell. Biol.* **14**, 5182–5191.
Waterman, J. L., Shenk, J. L. & Halazonetis, T. D. (1995). *EMBO J.* **14**, 512–519.
Wong, K. B., DeDecker, B. S., Freund, S. M., Proctor, M. R., Bycroft, M. & Fersht, A. R. (1999). *Proc. Natl Acad. Sci. USA*, **96**, 8438–8442.
Zhang, W., Guo, X. Y. & Deisseroth, A. B. (1994). *Oncogene*, **9**, 2513–2521.
Zhao, K., Chai, X., Johnston, K., Clements, A. & Marmorstein, R. (2001). *J. Biol. Chem.* **276**, 12120–12127.